Measurement of surface displacements in 1-3 and 1-1-3 piezocomposites

L. Li and N. R. Sottos[a)]
Department of Theoretical and Applied Mechanics, University of Illinois at Urbana-Champaign, Urbana, Illinois 61801

(Received 14 August 1995; accepted for publication 30 October 1995)

In a piezoelectric ceramic–polymer composite, the piezoceramic and the nonpiezoelectric polymer will have different deformations when subjected to an external electrical or mechanical stimulus. This local, nonuniform deformation eventually determines the overall electromechanical behavior of the composite. In the current investigation, static surface displacements of piezocomposites with 1-3 and 1-1-3 connectivity were measured using a scanning heterodyne laser interferometer. The influence of a thin interlayer surrounding the piezoceramic rods on the resulting displacement profiles was investigated and correlated with rod/polymer adhesion. The elastic stiffness of the interlayer as well as the interfacial adhesion had a significant effect on the rod displacement. Rods coated with a very compliant interlayer had a much larger displacement than untreated rods, while rods treated with a silane coupling agent to enhance adhesion had a much lower displacement. Experimental displacement profiles were found to be in good agreement with theoretical predictions. © *1996 American Institute of Physics.* [S0021-8979(96)07603-4]

I. INTRODUCTION

Piezocomposites are candidates for sensors and actuators in adaptive material systems. In particular, type 1-3 piezocomposites have demonstrated higher sensitivity and improved hydrostatic piezoelectric properties. These composites are named for their connectivity and consist of aligned, piezoceramic rods embedded in a passive polymer matrix. The addition of a third phase or interlayer around the piezoceramic rods, shown schematically in Fig. 1, results in a composite with 1-1-3 connectivity. Recent theoretical work by the authors[1] and experimental studies by Kim, Rittenmyer, and Kahn[2] have demonstrated significant increases in hydrostatic sensitivity with a 1-1-3 configuration.

In a 1-3 or 1-1-3 piezocomposite, the piezoceramic rod and the nonpiezoelectric polymer will have different deformations when subjected to an external electrical or mechanical stimulus. The deformation of each constituent depends on the relative compliance of the ceramic and matrix phases and any interlayer existing between them. This local, nonuniform deformation eventually determines the overall electromechanical behavior of the composite. For example, the average out-of-plane surface displacement can be correlated with the effective piezoelectric d_{33} constant for the composite. Thus, it is important to understand the local interaction between the piezoceramic and polymer matrix, especially near the ceramic/polymer interface.

Experimental characterization of piezocomposites can be roughly divided into two categories. Associated with the first category are measurements of dielectric and piezoelectric constants using the direct piezoelectric effect or the resonance method outlined in the IEEE Standard on Piezoelectricity.[3] Wang and Auld[4] and Gururaja *et al.*[5] measured surface displacement at resonance frequencies using heterodyne interferometry. Klicker[6] used a Berlincourt piezo d_{33} meter to measure the d_{33} value at different locations on the surface of 1-3 piezocomposites. The effective $\bar{d}_{33}$ piezoelectric constant of the composite was then taken to be the average of all the measured values. Klicker also measured the effective hydrostatic piezoelectric constant $\bar{d}_h$ by employing a static technique based on the direct effect. Using a similar method, Kim and co-workers[2] determined the effective $\bar{d}_h$ for several 1-1-3 piezocomposite configurations.

To measure the piezoelectric properties over broad ranges of frequency, nonresonance measurement techniques must be used. Consequently, the second category of experimental characterization involves measuring surface velocity and displacement at a certain frequency by laser probing methods. Rittenmyer and Dubbelday[7] reported a direct measurement of the effective, temperature-dependent piezoelectric coefficients by laser Doppler vibrometry. Zhang *et al.*[8] measured the surface displacement profile of a 2-2 piezocomposite at low frequency (200 Hz) with a double-beam laser dilatometer. The low-frequency performance of a single rod piezocomposite was investigated by Sottos *et al.*[9] using a laser heterodyne interferometer.

Although measurements of very low frequency ($<$100 Hz) or static displacements in 1-3 and 1-1-3 piezocomposites have not been reported previously in the literature, theoretical predictions of static displacements have been derived by several researchers. Cao, Zhang, and Cross[10] developed a one-dimensional model to predict the displacement profile of a piezoceramic rod or tube and surrounding polymer matrix when driven by an external electric field. More recently, the authors[11] used a three-phase composite cylinder model to calculate the nonuniform displacement profile in a single rod piezocomposite. Predictions of the local deformations were highly sensitive to the piezoelectric properties of the rod and the elastic properties of the polymer. The properties of the interface region between the rods and the matrix were also shown to have a significant effect on local behavior. In the current study, the *in situ* static displacements of piezocomposites with 1-3 and 1-1-3 connectivity are measured using heterodyne interferometry. In particular, the influence of a

a)Electronic mail: n-sottos@uiuc.edu

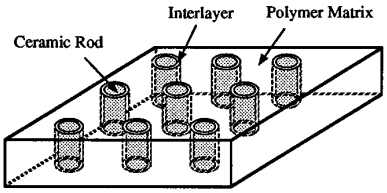

FIG. 1. Schematic of a 1-1-3 piezocomposite.

distinct interlayer on the displacement profiles is investigated and correlated with the rod/polymer adhesion. The experimental displacement values are compared to predictions by the authors.[11]

II. MICROINTERFEROMETRIC METHOD

Quantitative analysis of the local static deformations in 1-3 piezoceramic–polymer composites is a challenging problem. Since the deformations are small and nonuniform, the experimental technique must have an out-of-plane sensitivity of approximately 5 nm and a spatial resolution commensurate with the dimensions of the composite unit cell. Previous investigations by Sottos, Scott, and McCullough[12] and Ryan, Scott, and Sottos[13] have demonstrated the utility of heterodyne microinterferometric methods for nondestructively measuring displacements in the interfacial regions of polymer matrix composites. Because a long distance microscope with a high magnification is used, the interferometer probe has the capability to resolve small displacements in a very small region. The current investigation adapts this microinterferometric technique for measuring static surface displacements in 1-3 and 1-1-3 piezocomposites.

A. Apparatus

A scanning heterodyne microinterferometer similar to that described in detail by Sottos and co-workers[12] is utilized to measure the surface displacements of single rod piezocomposite samples. A single frequency, linearly polarized light beam of wavelength 514.5 nm from an argon laser (Lexel Laser model 3500) is incident upon a 40 MHz acousto-optic modulator (AOM) producing two beams which are sent along different arms of the interferometer. The first beam is shifted in frequency by 40 MHz and is used as a reference beam. The second beam with the same frequency as the beam incident upon the AOM is used to illuminate the sample surface. Hence, the sample serves as a mirror in this arm of the interferometer. The sample is mounted on a translation and rotation stage, such that only the outer edges of the back face of the sample are actually touching the fixture. This arrangement allows the sample to displace freely. The sample is manually adjusted for angular tilt when aligning the interferometer.

The two beams are recombined in a beam splitter and then arrive at the primary lens of a long distance microscope (Infinity model K2) placed before an eyepiece lens. An image (interferogram) of the sample surface is magnified onto the image plane with this long distance microscope, where a scanning photodiode detector scans the magnified image.

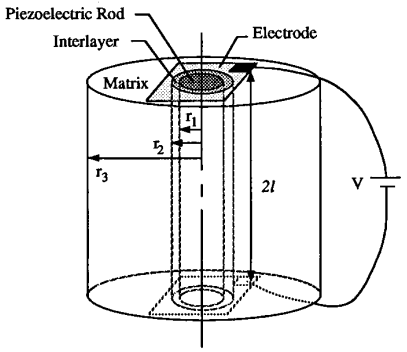

FIG. 2. Schematic of single rod sample for interferometric measurements.

The large numerical aperture of the long distance microscope increases light gathering power and permits high-resolution imaging. Through the use of different lenses, magnifications from 1× to 100× are attainable. Depending on the magnification of the image, the in-plane resolution is limited either by the optical system or by the diameter of the detector window.

A dynamic image which travels at a 40 MHz beat signal across the image plane is formed because of the difference in frequency between the sample and reference beams. One corner of the image plane is reflected by a mirror onto a second photodetector. The signal at this stationary photodetector is used as a phase reference signal. The phase of the image signal is continuously compared with phase of the reference signal. As a result, such dynamic disturbances as air turbulence, mechanical vibration, and thermal drift, that occur within the interferometer but away from the sample, do not affect the measurements.

The scanning photodiode detector is moved across the magnified sample image using two actuators which are perpendicular to each other. The actuators (Newport model 850B) are controlled by a microcomputer-controlled motion controller (Newport model PMC200P). A high-frequency lock-in amplifier (EG&G PARC model 5202) is used to measure the phase of the image signal. The output signal from the lock-in amplifier is digitized by a digital oscilloscope (Tektronix model TDS 420). Both the oscilloscope and the motion controller are interfaced with a central control unit, a Power Macintosh (Apple model 8100/80) via the IEEE-488.2 interface. The sweep rate of the oscilloscope is synchronized to the scanning of the photodetector by a virtual instrument (VI) written in LABVIEW (National Instruments) graphic language.

B. Sample fabrication

The interferometer is used to measure the static deformations resulting from activating a single PZT rod embedded in a polymer matrix. A schematic of the specimen is shown in Fig. 2. The piezoceramic (PZT) rods produced by Ceramic Processing Systems were 1 mm in diameter and poled in an oil bath under an electric field of 20 kV/cm. The axial piezoelectric constant was measured as $d_{33}=420\times10^{-12}$ m/V. For the matrix, a Shell EPON-828 epoxy resin with a Shell DETA curing agent was chosen. The samples were fabricated

TABLE I. Spurr epoxy compositions.

Coating	VCD (g)	DER (g)	NSA (g)	DMAE (g)
Type I	10	6	26	0.4
Type II	10	9.1	26	0.4
Type III	10	19.6	26	0.4

by placing a PZT rod into the center of a mold which was then filled with epoxy. The samples were cured at room temperature for 7 days and postcured at 40 °C for 4 h to raise the glass transition temperature of the epoxy.

The influence of a distinct interlayer between the rod and the polymer was investigated by fabricating samples with several different interface conditions. In the first type (I), the rods were embedded with no special interface treatment or coating as described above. In the second type (II), a thin polymeric coating with a Young's modulus lower than that of the bulk matrix was applied to the rods prior to being embedded. Type-III samples had an even lower modulus (almost rubberlike) coating applied to the rods. Finally, for the fourth sample type (IV), the rods were treated with a silane coupling agent obtained from Fiber Materials, Inc.

Spurr epoxy (Polysciences) was used for the compliant coatings (types II and III). Spurr epoxy is a four-component system. The modulus was varied by changing the concentration of the flexibilizer, diglycidyl ether of polypropylenglycol (DER), in the stoichiometric mix. Table I lists the various compositions of Spurr used in this study and the designation of each composition. Coatings were applied by dipping the rods in the epoxy and curing at 70 °C for 8 h. To increase the thickness, a second layer of coating was applied to the first layer. Properties of the coatings as measured by uniaxial tension tests are listed in Table II.

III. INTERFACIAL ADHESION

It is essential to have some measure of the interfacial bond strength between the coated PZT rods and the polymer matrix for the evaluation of mechanical response and the development of well-designed interfaces. Displacement measurements are sensitive to the PZT polymer adhesion as well as the elastic properties of the coating. Although the literature abounds with studies of fiber/matrix adhesion in polymer composites, very little work has been carried out on piezoceramic/polymer adhesion.

A thin-section push-out test was developed to measure the PZT rod/polymer interface strength.[14] This test, which has been used extensively to measure the *in situ* interfacial shear strength in fibrous composites, is useful for evaluating

TABLE II. Properties of the Spurr epoxy coatings.

Coating	Young's modulus $Y^{(2)}$ (GPa)
Type I	2.1
Type II	0.6
Type III	0.01

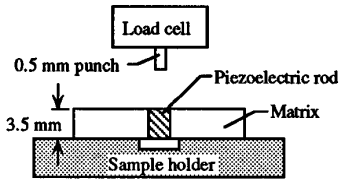

FIG. 3. Schematic of the thin section push-out test.

the effects of coatings on debonding. A schematic of the thin-section push-out apparatus is shown in Fig. 3. Single rod samples as described above were cut to a length of approximately 3.5 mm. Tests were conducted by applying an axial load to the rod using a punch which is attached to an Instron testing machine. A constant cross-head displacement rate of 0.05 mm/s was used for the tests. A typical load versus displacement curve is shown in Fig. 4. The maximum load corresponds to the point at which the rod debonded from the matrix. Using the maximum load $P_{\max}$ and the sample dimensions, the average interfacial shear strength τ_0, was calculated using the equation

$$\tau_0 = \frac{P_{\max}}{4\pi r_1 l}. \tag{1}$$

Although this simplified equation only calculates an average interfacial strength, it is useful for comparing adhesion changes due to the different interlayers or surface treatments used in this study. The effects of different coating types on interfacial shear strength are summarized in Table III. The results show that the addition of an interlayer with lower elastic modulus has almost no effect on the average interfacial shear strength at room temperature. The results also show that the interfacial shear strength is significantly increased by the silane coupling agent.

IV. DISPLACEMENT MEASUREMENTS

For the interferometric experiments, single rod samples were cut to a length of 5 mm and the front face finely polished. Polishing of the face on which the laser probe measurements are made was critical to insure a flat surface free of scratches. After polishing a thin gold coating was evaporated on the front surface of the sample to provide a highly reflective surface for the interferometric measurement as

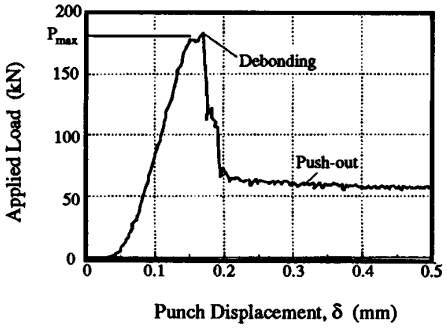

FIG. 4. A typical load-displacement curve for the push-out test.

TABLE III. Average interfacial shear strength for the different coatings.

Coating	Interfacial shear strength (MPa)
Type I	17.3
Types II and III	18.7
Type IV	22.4

well as an electrode for applying the electric field. Silver paint was applied to the back surface of the sample to provide a second electrode.

The piezoceramic rod was actuated by applying a static voltage across the piezocomposite sample. Two types of displacement measurements are reported below. In the first type of measurement, maximum displacement is recorded as a function of time after actuation. In the second type of measurement, displacement profiles of the single-rod composite are obtained.

A. Maximum surface displacement

Previous theoretical studies predict that the maximum displacement will occur at the center of the ceramic rod.[11] Consequently, the scanning detector in the experiments is fixed at the center of the PZT rod to measure the maximum displacement. An electric field is applied across the sample, which triggers the acquisition of the phase data as the sample responds. The phase change is then converted to displacement for that particular point. Measured displacements are plotted as a function of time for all four types of samples in Fig. 5. The applied voltage is also shown in this figure. The displacement at the center of the PZT rod jumps rapidly in about 400 ms from zero to its stable value when the dc voltage is turned on.

The displacements of the samples with a low-modulus interphase (types II and III) were higher than that of the untreated samples (type I). Because the adhesion between the Spurr epoxy coated rods is almost the same as that of the untreated rods (see Table III), the increase in displacement is

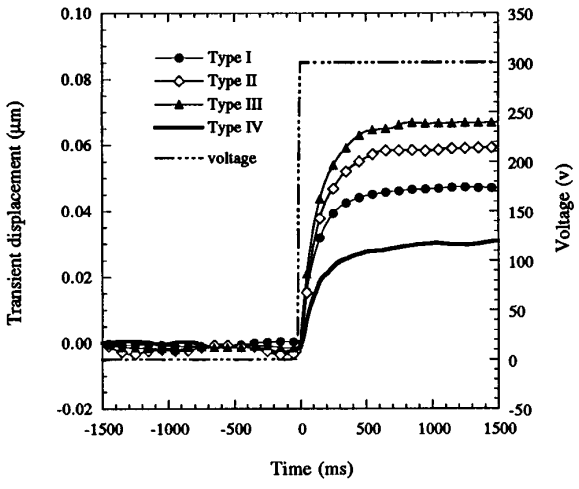

FIG. 5. Transient displacements measured at the center of the PZT rod.

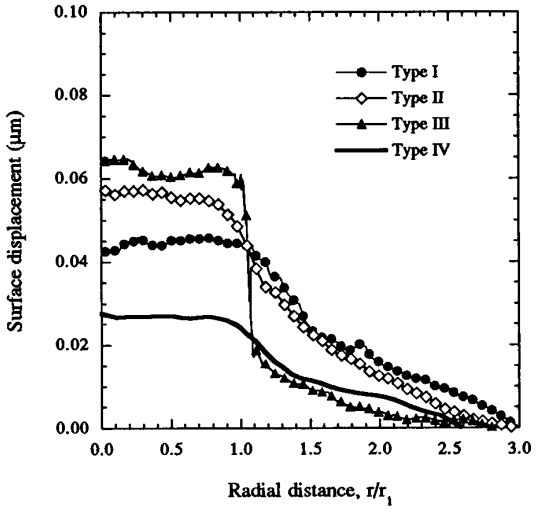

FIG. 6. Displacement profiles measured across the composite sample surface.

due solely to the reduction in stiffness of the interlayer surrounding the rod. The samples treated with a silane coupling agent (type IV) had a lower displacement than the untreated samples (type I). This decrease in displacement may be attributed to the increase in adhesion between the silane treated rod and the surrounding matrix or to the formation of a stiffer interlayer near the rod due to a reaction between the silane coupling agent and the matrix during sample cure. The extent of reaction of the silane with the matrix is not well known and therefore makes it very difficult to assess the properties near the rod surface.

B. Surface displacement profile

Surface displacement profiles are obtained by scanning the detector in a radial path from the rod center. To measure the net displacements of the sample, an initial scan of the surface is made before activation. The sample is then activated and a second scan is run. During each scan, phase data are continuously recorded and stored. Displacements are calculated by subtracting the phase data of the initial scan lines from the final ones. All out-of-plane displacements are measured relative to the same reference point, which is at a distance three times the rod radius away from the rod center.

In Fig. 6 axial displacement is plotted as a function of radial distance for each type of sample. The displacement over the surface is nonuniform with the maximum occurring in the PZT rod and decreasing rapidly with increasing radial distance into the matrix. The displacement profile is significantly influenced by the different coatings applied to the rod. Sample type III with the most compliant coating showed the highest rod displacement and also the greatest nonuniformity in the displacement profile across the surface. Sample type II also had a greater rod displacement than the untreated sample, but a much more similar profile in the matrix. The silane treated sample (type IV) had the smallest rod displacement but the most uniform profile. Hence, the addition of a

TABLE IV. Elastic properties of PZT rods.

Elastic constants (GPa)	PZT
$c_{11}^{(1)}$	126
$c_{12}^{(1)}$	79.5
$c_{13}^{(1)}$	84.1
$c_{33}^{(1)}$	117
$c_{44}^{(1)}$	23.0

thin compliant interlayer region effectively decouples the rod from the matrix leading to an increase in rod displacement and nonuniformity of the displacement profile. On the other hand, samples treated with a silane coupling agent to enhance adhesion have smaller and more uniform surface displacements.

V. COMPARISON OF THEORETICAL AND EXPERIMENTAL DISPLACEMENTS

The authors[11] derived theoretical predictions of static displacements in 1-1-3 piezocomposites using a three-phase composite cylinder model. This model accounts for the finite aspect ratio of the rods as well as the properties of a distinct interface region surrounding the rods. The expression for axial displacement of the components is given by[11]

$$w_c^{(i)}=\sum_{n=1}^{\infty}\sin(\mu_n z)[A_{1n}^{(i)}h_{3n}^{(i)}(r)+A_{3n}^{(i)}h_{4n}^{(i)}(r)+A_{2n}^{(i)}g_{3n}^{(i)}(r)+A_{4n}^{(i)}g_{4n}^{(i)}(r)]+B^{(i)}z, \tag{2}$$

where $i=1$, 2, and 3 for the piezoceramic rod, the interface region, and the matrix, respectively. The sets of constants $A_{1n}^{(i)}$, $A_{2n}^{(i)}$, $A_{3n}^{(i)}$, and $A_{4n}^{(i)}$ are determined from the boundary conditions on the cylinder and the functions $h_{3n}^{(i)}(r)$, $h_{4n}^{(i)}(r)$, $g_{3n}^{(i)}(r)$, and $g_{4n}^{(i)}(r)$ are expressed,

$$h_{3n}^{(i)}=\left(\frac{1}{c_{11}^{(i)}-c_{12}^{(i)}}\right)\mu_n^2 I_0(\mu_n r), \tag{3}$$

$$h_{4n}^{(i)}=\left(\frac{\mu_n^2}{c_{11}^{(i)}-c_{12}^{(i)}}\right)\left(\frac{4c_{11}^{(i)}}{c_{11}^{(i)}+c_{12}^{(i)}}I_0(\mu_n r)+\mu_n r I_1(\mu_n r)\right), \tag{4}$$

$$g_{3n}^{(i)}=\left(\frac{1}{c_{11}^{(i)}-c_{12}^{(i)}}\right)\mu_r^2 K_0(\mu_n r), \tag{5}$$

$$g_{4n}^{(i)}=\left(\frac{\mu_n^2}{c_{11}^{(i)}-c_{12}^{(i)}}\right)\left(\frac{-4c_{11}^{(i)}}{c_{11}^{(i)}+c_{12}^{(i)}}K_0(\mu_n r)+\mu_n r K_1(\mu_n r)\right), \tag{6}$$

TABLE V. Materials properties for EPON 828 epoxy.

Young's modulus $Y^{(3)}$ (GPa)	Poisson's ratio $\nu^{(3)}$
2.5	0.3

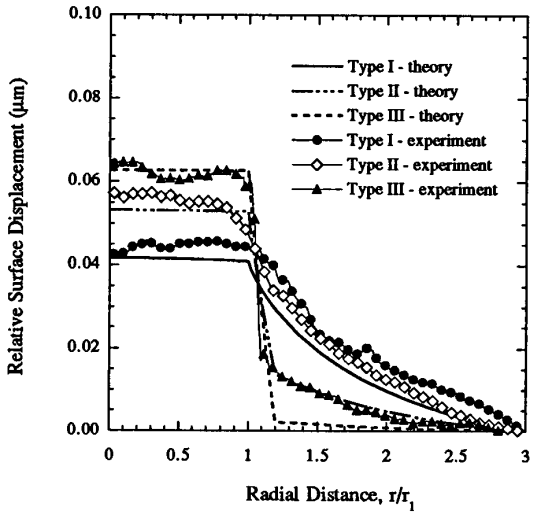

FIG. 7. Comparison of theoretical and experimental displacement profiles.

where I_0, I_1 and K_0, K_1 are the modified Bessel functions of the first and second kind and $c_{ij}^{(i)}$ are the elastic stiffness constants for each constituent.

The constants s_j $(j=1,2)$ are determined by

$$s_j=\frac{p_j^2 c_{11}^{(1)}-c_{44}^{(1)}}{c_{13}^{(1)}+c_{44}^{(1)}} \quad (j=1,2), \tag{7}$$

where p_1^2 and p_2^2 are the roots of the following equation:

$$c_{11}^{(1)}c_{44}^{(1)}p^4+[c_{13}^{(1)}(c_{13}^{(1)}+2c_{44}^{(1)})-c_{11}^{(1)}c_{33}^{(1)}]p^2+c_{33}^{(1)}c_{44}^{(1)}=0. \tag{8}$$

The μ_n are the eigenvalues and determined by the boundary conditions to be

$$\mu_n=\frac{n\pi}{2l} \quad (n=1,3,5,\ldots). \tag{9}$$

A one-to-one comparison of theory and experiment is difficult because the exact thicknesses of the coatings are unknown and many of the properties of the piezoceramic rod had to be taken from manufactured published values; however, trends in the variation of surface displacement profile due to changes in interlayer properties can still be assessed. Predictions of the surface displacement profile are determined from Eqs. (2)–(9). For the calculations, the measured value of $d_{33}=420\times10^{-12}$ m/V is used and the value of d_{31} is estimated to be $d_{31}=-198\times10^{-12}$ m/V. Elastic properties for the PZT rod are listed in Table IV as specified by Morgan Matroc, Inc.[15] Materials properties for EPON 828/DETA epoxy were measured using uniaxial tension tests and are listed in Table V. Geometric parameters are $r_1=0.5$ mm, $r_2=0.6$ mm, $r_3=3.0$ mm, and $l=2.5$ mm.

Theoretical displacement profiles for samples with no interlayer (type I) and a low modulus interlayer (types II and III) are plotted in Fig. 7 for an applied dc voltage of 300 V. The experimental profiles for these sample types have also been included in Fig. 7. Because the interferometric tech-

nique measures displacement relative to a reference point, the theoretical displacements must also be plotted relative to the experimental reference point. Consequently, all of the displacements in Fig. 7 are relative to the reference displacement at $r=3r_1$. The theoretical prediction of displacement for the untreated rod (type I) is slightly less than the experimental value, but overall the variations of surface displacement profile due to changes in interlayer properties are in good agreement with the experimentally observed trends. No predictions were made for the silane treated sample (type IV) since the properties and thickness of the interface region in this case are not known.

VI. DISCUSSION AND CONCLUSIONS

Microinterferometric measurements as well as the theoretical predictions demonstrate that the out-of-plane displacements of 1-1-3 piezocomposites are highly dependent on the interaction between the polymer matrix, a thin interlayer, and the piezoelectric ceramic. By introducing a thin compliant interlayer, the out-of-plane displacement of the rod is greatly increased while the requirement for overall stiffness of the composite can still be satisfied. The interlayer essentially serves to couple or decouple the rods from the matrix, depending on the interlayer stiffness. The application of a silane coupling agent to the rods improves interfacial adhesion and reduces the nonuniformity of the displacement profile in the whole composite region.

The measured displacement profile can also be used to estimate the effective piezoelectric $\bar{d}_{33}$ constant of the composite. For thin section 1-3 piezocomposites, $\bar{d}_{33}$ can be calculated from the out-of-plane displacement as

$$\bar{d}_{33}=\frac{1}{\Omega}\int \frac{2w(x,y)}{V}\,d\Omega, \tag{10}$$

where V is the voltage applied and the integral is over the area Ω measured on the surface of the composite sample. Because only single rod samples were tested in the current study, the rod volume fractions are too low to calculate an effective $\bar{d}_{33}$ value for the sample using Eq. (10); however, the experimental technique could be applied to measure the displacement of a rod in a larger array to determine the $\bar{d}_{33}$ of the piezocomposite.

Because the properties of the interlayer alter the displacement profile, the interlayer should also have a significant influence on the effective properties of the piezocomposite. As mentioned previously, theoretical work by the authors[1,11] and experimental studies by Kim and co-workers[2] have demonstrated that the properties of a distinct interlayer significantly affect the performance of a piezocomposite. Both the effective $\bar{d}_{33}$ and $-\bar{d}_{31}$ were shown to decrease with increasing interlayer compliance.[11] However, the effective hydrostatic piezoelectric constant, $\bar{d}_h=\bar{d}_{33}+2\bar{d}_{31}$, will increase with increasing interlayer compliance because the decrease in $-2\bar{d}_{31}$ is larger than the corresponding decrease in $\bar{d}_{33}$.[1] Thus, the properties of the interlayer can be tailored to optimize piezocomposite performance.

ACKNOWLEDGMENTS

The support of the Office of Naval Research under contract monitor Roshdy Barsoum is greatly appreciated. The assistance of Kathleen Durkin in carrying out the push-out experiments is also gratefully acknowledged.

[1] L. Li and N. R. Sottos, J. Appl. Phys. **77**, 4595 (1995).
[2] C. Kim, K. M. Rittenmyer, and M. Kahn, Ferroelectrics **156**, 19 (1994).
[3] Institute of Electrical and Electronics Engineers (IEEE), "IEEE Standard on Piezoelectricity," IEEE Std. 176-1978 (1978).
[4] Y. Wang and B. A. Auld, in Proceedings of the 1985 IEEE Ultrasonic Symposium, San Francisco, 1985, p. 637.
[5] T. R. Gururaja, W. A. Schulze, L. E. Cross, L. E. Cross, R. E. Newnham, B. A. Auld, and Y. J. Wang, IEEE Trans. Sonics Ultrason. **SU-32**, 481 (1985).
[6] K. A. Klicker, Ph.D. thesis, The Pennsylvania State University, State College, PA, 1980.
[7] K. M. Rittenmyer and P. S. Dubbelday, J. Acous. Soc. Am. **91**, 2254 (1992).
[8] Q. M. Zhang, W. Cao, J. Zhao, and L. E. Cross, IEEE Trans. Ultrason. Ferroelectrics Frequency Control **41**, 556 (1994).
[9] N. R. Sottos, L. Li, W. R. Scott, and M. J. Ryan, Proc. SPIE **1916**, 87 (1993).
[10] W. Cao, Q. M. Zhang, and L. E. Cross, J. Appl. Phys. **72**, 5814 (1992).
[11] L. Li and N. R. Sottos, J. Intelligent Mater. Sys. Struct. **6**, 169 (1995).
[12] N. R. Sottos, W. R. Scott, and R. L. McCullough, Experimental Mech. **31**, 98 (1991).
[13] M. J. Ryan, W. R. Scott, and N. R. Sottos, *Review of Progress in Quantitative Nondestructive Evaluation* (Plenum, New York, 1990).
[14] L. Li, K. M. Durkin, and N. R. Sottos, in *Proceedings of The American Society for Composites Ninth Technical Conference* (Technomic, Lancaster, 1994), p. 5.
[15] Morgan Matroc, Inc., *Piezoelectric Technology Data for Designers* (Morgan Matroc, Bedford, 1989).